Optics Letters

Measurement of the birefringence variation induced by dihydrogen diffusion into a polarization-maintaining fiber

Mohamed Aazi,[1,2] Damien Kinet,[2] Claude Renaut,[3] Johan Bertrand,[4] Jean-Louis Auguste,[1] Patrice Mégret,[2] and Georges Humbert[1,*]

[1]*XLIM Research Institute, UMR 7252 CNRS/Limoges University, 123 Av. A. Thomas, Limoges, France*
[2]*Electromagnetism and Telecommunication Department, Faculty of Engineering, University of Mons, Boulevard Dolez 31, 7000 Mons, Belgium*
[3]*ANDRA, French National Radioactive Waste Management Agency, Centre de Meuse/Haute-Marne, Route Départementale 960, BP 9, 55290 Bure, France*
[4]*ANDRA, French National Radioactive Waste Management Agency, Parc de la Croix Blanche, 1–7 Rue J. Monnet, Chatenay-Malabry, France*
*georges.humbert@xlim.fr

We report continuous measurements of the transmission spectrum of a fiber loop mirror interferometer composed of a Panda-type polarization-maintaining (PM) optical fiber during the diffusion of dihydrogen (H_2) gas into the fiber. Birefringence variation is measured through the wavelength shift of the interferometer spectrum when the PM fiber is inserted into a gas chamber with H_2 concentration from 1.5 to 3.5 vol.% at 75 bar and 70°C. The measurements correlated with simulation results of H_2 diffusion into the fiber lead to a birefringence variation of -4.25×10^{-8} per mol m^{-3} of H_2 concentration in the fiber, with a birefringence variation as low as -9.9×10^{-8} induced by 0.031 μmol m^{-1} of H_2 dissolved in the single-mode silica fiber (for 1.5 vol.%). These results highlight a modification of the strain distribution in the PM fiber, induced by H_2 diffusion, leading to a variation of the birefringence that could deteriorate the performances of fiber devices or improve H_2 gas sensors.   © 2023 Optica Publishing Group

The diffusion of H_2 gas into optical fibers has been thoroughly studied during the development of fiber Bragg gratings (FBGs) [1], due to the large improvement of the photosensitivity to UV radiations of standard single-mode telecommunication fibers (SMFs) when a fiber was exposed to high-pressure H_2 for several days or even weeks [2]. Knowledge of H_2 concentration in the fiber is important for controlling the photosensitivity, the fiber losses, the modification of photoelastic properties, and the augmentation of the refractive index leading to variations of the properties of fiber Bragg grating-based components after manufacturing [3–5]. More recently, Kong and Dong have developed a UV-post-processing technique based on the diffusion of H_2 into a polarization-maintaining (PM) SMF for locally modifying the acoustic velocity coefficient (by $\approx 2\%$), leading to a Brillouin frequency shift of up to -320 MHz, with a Brillouin frequency shift of around -2% per wt.% of OH level [6]. They demonstrated the possibility of using this technique to tailor the

acoustic velocity along a fiber for improving the suppression of the parasitic stimulated Brillouin scattering in a fiber amplifier. Delepine-Lesoille *et al.* have demonstrated Brillouin optical time-domain analyses of H_2 diffusion into a SMF, in distributed sensing configuration, with a Brillouin frequency shift of about 0.21 MHz per percent of H_2 concentration in the fiber [7]. Additional experiments based on simultaneous Brillouin and Rayleigh backscattering measurements during H_2 outgassing from H_2-loaded SMF (at saturation) have demonstrated a variation of the acoustic velocity of 5.2 m s^{-1} per mol% H_2 dissolved in silica and of the refractive index of silica of about 9.7×10^{-4} RIU per mol% H_2 dissolved in silica [8]. These results allow the development of distributed fiber sensors for remote monitoring of slow variation of H_2 concentration in H_2-rich atmospheres, as for high-level and long-lived intermediate-level radioactive waste repositories. In contrast to most H_2 fiber sensors that are based on a deposited thin layer of a sensitive material [e.g., palladium (Pd) and tungsten oxide (WO_3) [9–13]], raw-fiber-based distributed sensors offer remote, robust, long-term, and H_2 sensing in long-range structures in harsh and explosive conditions. They do not undergo delamination or cracking of the sensitive layer that could lead to severe stability problems [14,15]. However, SMFs suffer from a low H_2 sensitivity, as the variation of the Brillouin frequency is about 21 MHz for a hydrogenation saturation at 25°C and 150 bar. With the prospect of gaining in sensitivity while protecting the sensing material to external deterioration, we have demonstrated that the insertion of Pd particles inside the stress-applying parts (SAPs) of a Panda-type PM-SMF leads to a variation of the fiber birefringence during H_2 diffusion [16]. This modified fiber improved the wavelength shift of the transmission spectrum of a fiber loop mirror (FLM) interferometer by 32% and reduced the response time by 50%, in comparison with the same PM-SMF without Pd particles. Both PM fibers were inserted within a FLM interferometer and put in a gas chamber fully filled (100%) with H_2 gas. Besides, in comparison with a FBG written in a SMF (also inserted in the gas chamber), we observed that both PM fibers exhibit a faster response time and a larger wavelength shift. These results
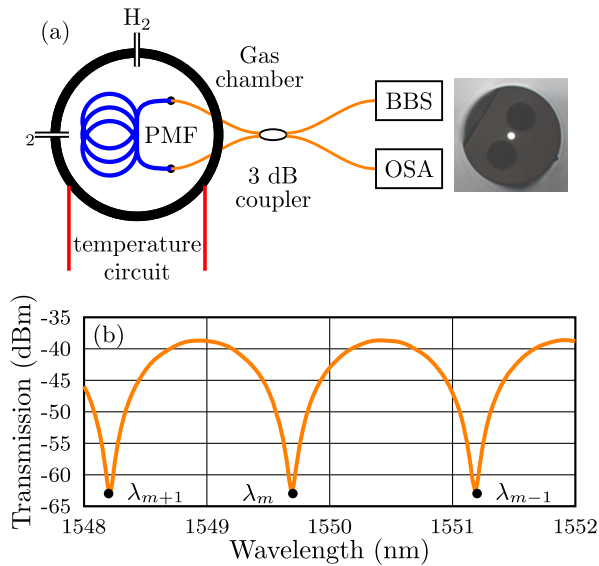
Fig. 1. (a) Experimental setup of the FLM interferometer hydrogen monitoring system based on commercial PM Panda fiber. (b) Transmission spectrum of the interferometer with a fiber length of 4 m.

associated with the large Brillouin frequency shift (-320 MHz) reported by Kong and Dong [6] in a PM-SMF (against 21 MHz in a SMF [7]) highlight a modification of the strain distribution in the PM-SMF, induced by H_2 diffusion, leading to significant variation of the fiber birefringence that could deteriorate the performances of devices or improve H_2 gas sensors.

In this paper, we explore this birefringence variation in a simple commercial PM-SMF (Thorlabs XP-1550, composed of boron-doped SAPs). We have designed an experimental setup to continuously measure the birefringence variation of PM fibers during diffusion of H_2 under controlled pressure and temperature. Different H_2 concentrations from 0.5 to 3.5 vol.% at 75 bar have been applied showing a birefringence variation of about -4.2×10^{-8} per mol m^{-3} of H_2 dissolved in silica.

The experimental setup used for continuously measuring the diffusion of H_2 into a PM-SMF, shown in Fig. 1(a), is composed of a hermetic gas chamber (volume of 2.5 l) with two channels for hydrogen (H_2) gas and nitrogen (N_2) gas flowing with controlled pressure and temperature.

The PM-SMF, spliced between two pigtails of SMF, is inserted into the chamber and connected through hermitic optical connectors to the arms of a SMF-based 3 dB coupler to form a FLM interferometer. An amplified spontaneous broadband light source (BBS; Amonics ALS-CL-17B-FA) with a central wavelength of around 1550 nm and a spectral bandwidth of 100 nm is used with an optical spectrum analyzer (OSA; Yokogawa AQ-6370, wavelength resolution of 0.05 nm) for measuring the transmission spectrum of the FLM. The PM fiber is a Panda-type fiber (Thorlabs XP-1550) with an inner cladding diameter of 125 µm and a core diameter of 8 µm. The SAPs are composed of boron-doped silica with a diameter of 36.5 µm distanced by 4.5 µm from the germanium-doped core center. The fiber has a core/cladding index difference of 5.5×10^{-3} and a SAP/cladding index difference value of -12×10^{-3}. A FLM interferometer is a sensitive configuration to many physical parameters, and in particular to the birefringence of a PM fiber [17,18]. The transmission spectrum $T(\lambda)$ of the FLM [Fig. 1(b)] depends on the

length L and on the group birefringence B of the PM fiber, as the incident light from the BBS is split into two beams of clockwise and anticlockwise propagations. Each of the resultant beams is decomposed into two polarization components after it travels through the high-birefringence fiber. The counter-propagating beams recombine at the output of the coupler and exhibit interference according to the phase difference induced by the birefringence. The output spectrum can be expressed as a sine-square function relative to the incident light wavelength [17]:

$$T(\lambda) = \sin^2 \frac{\pi BL}{\lambda}, \tag{1}$$

where λ is the wavelength. The dip wavelength λ_m in the interferometer spectrum [Fig. 1(b)] corresponds to $T(\lambda_m) = 0$ and is described as

$$\lambda_m = \frac{L}{m} B, \tag{2}$$

where m is an integer.

The measurement of the shift of the transmission spectrum (i.e., dip wavelengths λ_m) enables the sensing of tiny variations of the birefringence (B). The sensitivity is limited by the limit of detection of the wavelength shift that depends on the period of the interferences and the resolution of the OSA. As the length of the PM fiber has only an effect on the period of the interferences, a fiber length of 4 m was selected, leading to a FLM spectrum composed of 40 dips (within a wavelength range of 70 nm of the BBS) with a period of FWHM = 1.32 nm [Fig. 1(b)]. A resolution of 0.05 nm of the OSA was used for ensuring an efficient tracking of the wavelength dips, with measurements each minute. By (2), the measured birefringence of the PM fiber is estimated to be 4.33×10^{-4} at around 1550 nm at ambient temperature and pressure. The diffusion of H_2 inside the optical fiber is monitored by measuring each minute the transmission spectrum of the FLM and more precisely by tracking the shift of the dips. As these wavelength shifts are a consequence of the birefrigence variation, it is an indirect and accurate means of sensing H_2 diffusion into the fiber. The temporal evolution of H_2 diffusion through the cross section of an optical fiber (from the external boundary to the center) is expressed by Fick's law, leading to (3) for the H_2 concentration $[H_2]$ [19]:

$$\frac{\partial [H_2]}{\partial t} = D \left(\frac{\partial^2 [H_2]}{\partial r^2} + \frac{1}{r} \frac{\partial [H_2]}{\partial r} \right), \tag{3}$$

where D is the diffusion coefficient of H_2 into SiO_2, expressed for silica as [20]

$$D = 2.83 \times 10^8 \exp\left(-\frac{40190}{RT}\right), \tag{4}$$

where R is the universal gas constant and T the absolute temperature. It is worth noting that H_2 diffusion does not depend on the gas pressure, but on the temperature. Higher temperatures and smaller fiber diameters lead to faster H_2 diffusion in silica. The concentration of H_2 in silica at saturation ($[H_2]_{sat}$) is obtained from the solubility S of H_2 into SiO_2 by the relation [20]

$$[H_2]_{sat} = \frac{p_{H_2} S}{N_A} = \frac{p_{H_2}}{N_A} \times 71 \times 10^{21} \exp\left(\frac{8900}{RT}\right), \tag{5}$$

with N_A the Avogadro constant and p_{H_2} the partial pressure of H_2. It is clear that the concentration of H_2 at saturation is larger for
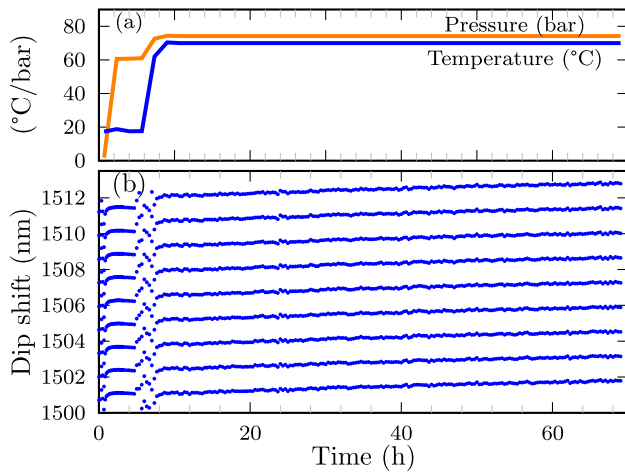
Fig. 2. (a) Pressure and temperature variations and (b) wavelength of spectrum dips during the calibration measurements with N_2 gas.

Fig. 3. Wavelength of spectrum dips during the hydrogenation protocol with 1.5 vol.% of H_2 gas.

Fig. 4. Normalized wavelength shift of the average interference dips during the hydrogenation protocol with different hydrogen concentrations (orange, 1.5 vol.%; blue, 2.5 vol.%; green, 3.5 vol.%).

Table 1. Summary of Results After Hydrogenation and Computed Values

$[H_2]/$ %	$p(H_2)/$ bar	$\frac{\Delta\lambda}{\lambda_0}$ (67 h) $\times 10^{-4}$	c (sat)/ mol m^{-3}	$\frac{\Delta\lambda}{\lambda_0}$ (sat) $\times 10^{-4}$	c (67 h)/ mol m^{-3}	ΔB (67 h) $\times 10^{-7}$
1.5	1.06	−2.39	2.76	−2.60	2.54	−0.99
2.5	1.77	−4.23	4.60	−4.60	4.23	−1.70
3.5	2.48	−6.25	6.45	−6.80	5.93	−2.52

lower temperature and/or higher pressure. Therefore, the temperature and the pressure of H_2 in the gas chamber were set at 70 °C and 75 bar, respectively. This enables a rather fast H_2 diffusion in the fiber samples until saturation with measurable H_2 concentration, which leads to the following experimental protocol. Measurement with N_2 gas was realized to calibrate the system. As shown in Fig. 2(a), the chamber was initially filled with ambient air at room temperature (17.5 °C), then N_2 was inserted at 60 bar (during 7 hours, for checking the hermiticity of the chamber), and finally the temperature and N_2 pressure were increased up to 70 °C and 75 bar, respectively. These conditions were maintained during 67 hours to enable slow dynamic measurements. Then the gas was released and the temperature was decreased to room temperature. Continuous measurements of the transmission spectrum of the FLM allow us to quantify a linear shift of the wavelength dips of 0.01 nm per hour [Fig. 2(b)] corresponding to the drift of the measurement system.

To monitor the diffusion of a given concentration of H_2 into the PM fiber, the chamber was initially filled with N_2 gas ($p = 60$ bar at room temperature, 18.5 °C) during a few hours to check again the hermiticity. Then, H_2 was injected in the gas chamber with a partial pressure corresponding to the desired H_2 concentration. Next, the temperature of the mixture ($N_2 + H_2$) was increased to 70 °C (leading to a pressure of 75 bar) Finally, after 67 hours in these conditions, the chamber was purged, opened, and the PM fiber was removed and replaced by a virgin one. This protocol was used for measuring the diffusion of H_2 at a concentration of 0.5, 1.5, 2.5, and 3.5 vol.%. Figure 3 shows the evolution of the dip wavelength of the FLM measured on-line each minute during this hydrogenation protocol for a gas chamber filled with N_2 gas mixed with 1.5 vol.% of H_2 gas.

By an appropriate calibration procedure, detailed in Supplement 1, we obtain the normalized wavelength shift [$(\lambda - \lambda_0)/\lambda_0$, with λ_0 the wavelength at the beginning of the hydrogenation stage] of the average interference dips versus the hydrogenation time plotted in Fig. 4, for different H_2 concentrations. The curves include the correction from the system calibration. They exhibit a continuous shift of the interference dip to shorter wavelengths following an exponential decay until a plateau corresponding to the saturation regime. As the kinetics of H_2 diffusion in this
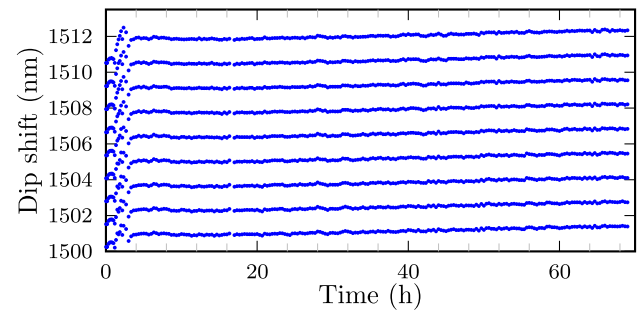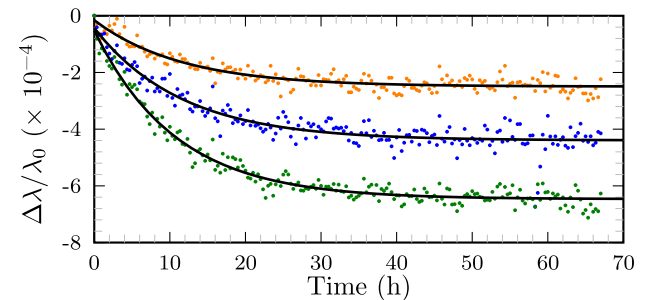
transient regime only depends on the temperature, we have simulated [from (3)] the normalized diffusion of 100% H_2 (at 70 °C) into the center of a silica cylinder of 125 µm in diameter, and then fitted the normalized wavelength shift of the average interference dips with this simulation curve by applying, for each concentration, a multiplication factor that corresponds to the mean normalized wavelength shift at saturation (column 5 in Table 1). Indeed, after 67 hours of hydrogenation at 70 °C the normalized concentration of H_2 is about 91.96% of the saturation stage. As shown in Fig. 4, these curves match the measured data emphasizing that the kinetics of H_2 diffusion into the fiber was correctly measured with this apparatus based on a Panda PM fiber. After 67 hours of hydrogenation in these conditions (75 bar and 70 °C), the mean normalized wavelength shift obtained from these curves is summarized in Table 1. The mean normalized wavelength shift at saturation (column 5 in Table 1) is also equal to the measured value (column 3 in Table 1) divided by 91.96%.

The concentration of H_2 in the fiber can be calculated at saturation (column 4 in Table 1) from (5) knowing the partial pressures for the different concentrations of H_2, following the hydrogenation protocol. This factor of 91.96% is also applied
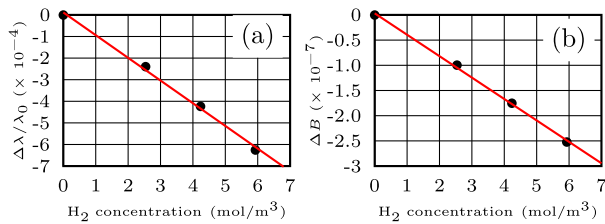
Fig. 5. (a) Normalized wavelength shift of interference dips and (b) birefringence variation versus the concentration of H_2 dissolved in silica.

to c(sat) for obtaining the concentration of H_2 in the fiber at the end of the hydrogenation process (column 6 in Table 1). It is worth noting that these concentrations correspond to 0.12, 0.21, and 0.29 µmol of H_2 in the 4 m long Panda fiber for the different hydrogenation concentrations of 1.5, 2.5, and 3.5 vol.% of H_2, respectively. Furthermore, these also correspond to a ratio of H_2 in silica of about 0.6×10^{-4}, 1.1×10^{-4}, and 1.5×10^{-4}, respectively. These calculations lead to plotting the mean normalized wavelength shift (at $t_{H_2} = 67$ h) versus the H_2 concentration at the same time [Fig. 5(a)] that is linearly fitted with a slope of -1.05×10^{-4} per mol m^{-3} and a standard error of 4.2×10^{-6}. Furthermore, (2) is linear in B, so that the normalized wavelength shift $\Delta\lambda/\lambda_0$ induced by a birefringence variation ΔB is simply expressed as

$$\frac{\Delta\lambda(t)}{\lambda_0} = \frac{\lambda(t) - \lambda_0}{\lambda_0} = \frac{\Delta B(t)}{B_0}, \qquad (6)$$

with B_0 the birefringence at the beginning of the hydrogenation stage, easily computed from the positions of λ_m at the initial time [see Fig. 5(b)]. The calculation of B_0 from the measured transmission spectrum of each experiment (at $t_{H_2} = 0$ h) leads to a birefringence variation at $t_{H_2} = 67$ h of about -9.9×10^{-8}, -1.7×10^{-7}, and -2.52×10^{-7}, respectively. These variations are linearly fitted versus the H_2 concentration in silica [Fig. 5(b)] with a slope of -4.25×10^{-8} per mol m^{-3} (with a standard error of 1.16×10^{-9}), which is equivalent to a birefringence variation of -7.43×10^{-8} per vol.% of H_2 in the chamber (with a standard error of 2.66×10^{-9}).

In conclusion, we have demonstrated continuous monitoring of H_2 diffusion into a commercially available Panda PM fiber within a FLM interferometer inserted in a gas chamber, with H_2 concentration from 1.5 to 3.5 vol.% at 75 bar and 70 °C. The evolution of the H_2 concentration in the fiber was obtained by correlating the simulation of the normalized diffusion of H_2 in the fiber core with the measurements of the wavelength shift of the FLM transmission spectrum. From these results we have demonstrated a birefringence variation of -4.25×10^{-8} per mol m^{-3} of H_2 concentration, with a birefringence variation as low as -9.9×10^{-8} induced by 2.54 mol m^{-3} of H_2 dissolved in silica (for 1.5 vol.%). As this result has been obtained at almost saturation ($t_{H_2} = 67$ h), smaller birefringence variation could be measured during the diffusion of H_2 into the fiber, which is emphasizes the sensitivity of this configura-

tion. Furthermore, this configuration does not require any fiber post-processing, fiber functionalization with a material sensitive to H_2, or a specific component. It is robust, of low cost, compact, easy to realize, and highly compatible with industrial applications that require the remote monitoring of slow leakage of H_2 (in harsh environments), such as within nuclear waste disposals. In addition, this experimental demonstration offers new insights for developing novel PM fibers with improved H_2 sensitivity.

Disclosures. The authors declare no conflicts of interests.

Data availability. Data underlying the results are not publicly available but may be obtained from the authors upon reasonable request.

Supplemental document. See Supplement 1 for supporting content.

REFERENCES

1. K. O. Hill, Y. Fujii, D. C. Johnson, and B. S. Kawasaki, Appl. Phys. Lett. **32**, 647 (1978).
2. P. J. Lemaire, R. M. Atkins, V. Mizrahi, and W. A. Reed, Electron. Lett. **29**, 1191 (1993).
3. P. L. Swart and A. A. Chtcherbakov, J. Lightwave Technol. **20**, 1933 (2002).
4. B. Malo, D. C. Johnson, F. Bilodeau, J. Albert, and K. O. Hill, Electron. Lett. **30**, 442 (1994).
5. S. R. Baker, H. N. Rourke, V. Baker, and D. Goodchild, J. Lightwave Technol. **15**, 1470 (1997).
6. F. Kong and L. Dong, Opt. Express **20**, 27810 (2012).
7. S. Delepine-Lesoille, J. Bertrand, L. Lablonde, and X. Pheron, IEEE Photonics Technol. Lett. **24**, 1475 (2012).
8. S. Leparmentier, J. L. Auguste, G. Humbert, G. Pilorget, L. Lablonde, and S. Delepine-Lesoille, Proc. SPIE **9634**, 963432 (2015).
9. M. Tabib-Azar, B. Sutapun, R. Petrick, and A. Kazemi, Sens. Actuators, B **56**, 158 (1999).
10. B. Xu, C. L. Zhao, F. Yang, H. Gong, D. N. Wang, J. Dai, and M. Yang, Opt. Lett. **41**, 1594 (2016).
11. M. Yang, Z. Yang, J. Dai, and D. Zhang, Sens. Actuators, B **166-167**, 632 (2012).
12. C. Caucheteur, M. Debliquy, D. Lahem, and P. Mégret, IEEE Photonics Technol. Lett. **20**, 96 (2008).
13. Y. Wang, M. Yang, G. Zhang, J. Dai, Y. Zhang, Z. Zhuang, and W. Hu, J. Lightwave Technol. **33**, 2530 (2015).
14. E. Lee, J. M. Lee, J. H. Koo, W. Lee, and T. Lee, Int. J. Hydrogen Energy **35**, 6984 (2010).
15. F. Greco, L. Ventrelli, P. Dario, B. Mazzolai, and V. Mattoli, Int. J. Hydrogen Energy **37**, 17529 (2012).
16. M. Aazi, M. Kudinova, D. Kinet, J.-L. Auguste, S. Delépine-Lesoille, P. Mégret, and G. Humbert, JPhys Photonics **2**, 014005 (2019).
17. Y. Liu, B. Liu, X. Feng, W. Zhang, G. Zhou, S. Yuan, G. Kai, and X. Dong, Appl. Opt. **44**, 2382 (2005).
18. A. N. Starodumov, L. A. Zenteno, D. Monzon, and E. D. L. Rosa, Appl. Phys. Lett. **70**, 19 (1997).
19. P. J. Lemaire, Opt. Eng. **30**, 780 (1991).
20. J. F. Shackelford, P. L. Studt, and R. M. Fulrath, J. Appl. Phys. **43**, 1619 (1972).